Rotordynamic Characteristics of an APU Gas Turbine Rotor-Bearing System Having a Tie Shaft

An Sung Lee*
Rotor Dynamics Group, Korea Institute of Machinery and Materials
Young-Seob Lee
Engine Engineering Center, Samsung Aerospace

In this paper it is intended to set-up a sound model of the 60,000 rpm 100 kW prototype APU gas turbine rotor-bearing system, and particularly to investigate the influences of the tie shaft on the rotordynamic characteristics of the entire APU gas turbine rotor-bearing system, employing the dual shaft model. Firstly, a mock-up APU rotor has been constructed to test and verify the model. Analytical natural frequency results have agreed with the corresponding modal test ones to within 5% difference. Then, the rotordynamic characteristics of the prototype APU rotor-bearing system have been investigated. Natural vibration and unbalance response analyses results have shown that the inner tie shaft resonance can cause high enough vibration of the outer main rotor shaft. This could be a concern as the rotor journals operate on very thin air film at high speed. It is concluded as a conservative design practice that the inner tie shaft should be explicitly modeled in the rotordynamic analysis of the APU rotor-bearing system.

Key Words : Rotordynamic, APU Gas Turbine, Rotor-Bearing System, Tie Shaft, Single Shaft Model, Dual Shaft Model, Finite Element Method

1. Introduction

In aeroengines or compact high performance gas turbines it is not unusual to find that their main rotors are made up of many segmented sections and that the rotors are tied as one piece by tie rods or tie shafts with high tensional axial preloads. These tie shafts and many discontinuous connections in general add some uncertainties and/or errors to analytical models of the rotors. In the gas turbine industries the mechanical integrities of such assembled systems are proved by dynamic tests on the rotors and tie shafts (Janssen and Joyce, 1996). However, any investigations addressing the tie shaft dynamics explicitly and its possible adverse influences on the main rotor are hardly found in open literatures.

In analyzing rotor-bearing systems the transfer matrix method (Pestel and Leckie, 1963; Koenig, 1961; Lund and Orcutt, 1967; Rao, 1983) and the finite element method (Ruhl and Booker, 1972; Zorzi and Nelson, 1977; Özgüven and Özkan, 1984; Lalanne and Ferraris, 1990) have been widely used. Generally speaking, the former is more advantageous in element formulations and computation times than the latter but more disadvantageous in modeling complex configurations and solution procedures. With rapid technological advances in the computer hardware the finite element method is gaining more popularity as a rotordynamic analysis tool these days.

In this study it is intended to set-up a sound model of the 60,000 rpm 100 kW prototype APU (auxiliary power unit) gas turbine rotor system shown in Fig. 1. It has a main outer shaft, which is composed of a number of segmented sections for manufacturing and assembly conveniences.

* Corresponding Author,
E-mail : aslee@mailgw.kimm.re.kr
TEL : +82-42-868-7356 ; **FAX** : +82-42-868-7440
Rotor Dynamics Group, Korea Institute of Machinery and Materials, Daejon 305-600, Korea. (Manuscript **Received** March 8, 2000; **Revised** July 5, 2000)

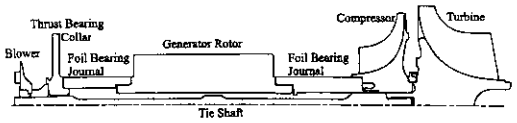

Fig. 1 Schematic of the 100 kW prototype APU rotor

For a secure assembly of the segmented sections a tie shaft or inner shaft is installed inside of the outer shaft and a tensional axial preload of 50,000 N is provided to it. The rotor system is modeled with the finite element method, considering the inner shaft dynamics explicitly by the dual shaft model. As the rotor journals supported by air-foil bearings in the present APU operate on very thin air film, any dynamic effect of the inner shaft on the outer main rotor shaft needs to be thoroughly reviewed during design stage. Firstly, a mock-up APU rotor is constructed to test and verify the model, especially connections of the segmented shafts. Then, the rotordynamic characteristics of the prototype APU rotor-bearing system are investigated with particular emphasis on evaluating the influences of the inner tie shaft on the rotordynamic behaviors of the outer main rotor shaft.

2. Rotor Modeling

The APU rotor-bearing system is modeled with the finite element method. The employed shaft element coordinate system is shown in Fig. 2, and the finite element formulation and solution procedures used in the coding are given in the Appendix.

In the modeling two models are considered. One is the conventional single shaft model, where the stiffness and inertia matrices of the inner shaft are added to the corresponding matrices of the outer shaft. The other is the dual shaft model, where the inner shaft is provided at its each node with independent degrees of freedom apart from those of the outer shaft. The tensional axial force on the inner shaft and the compressional axial force on the outer shaft are also considered in the models. The effects of such axial forces on the stiffness matrix of a shaft element are reflected in

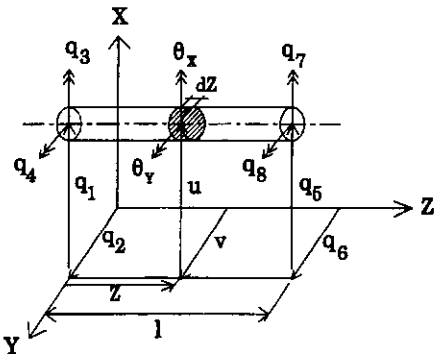

Fig. 2 Shaft element and its generalized displacements

Fig. 3 Schematic of the mock-up APU rotor for model verification

the model by considering the strain energy,

$$U_A = \pm\frac{1}{2}F_A\int_0^l\left[\left(\frac{\partial u}{\partial Z}\right)^2+\left(\frac{\partial v}{\partial Z}\right)^2\right]dZ \quad (1)$$

where F_A is an axial force acting on the shaft element, and + : tensional force and − : compressional force.

3. Results and Discussions

3.1 Mock-up APU rotor

Figure 3 shows a schematic of the mock-up APU rotor. It has been constructed at the early stage of design process to prove the handling of connections of segmented outer shaft sections and to verify the developed FE code. Its outer main rotor shaft is composed of a LHS bearing journal shaft, generator rotor, RHS bearing journal shaft built with a compressor wheel, and turbine wheel. The mechanical integrity of the outer shaft is sustained by the inner tie shaft, which is tensioned with an axial preload of 50,000 N. However, the mock-up APU rotor does not represent an exact equivalence to the prototype APU rotor as the latter has been finalized after several design modifications. To simulate soft-bearing supports the mock-up rotor has been placed on a sponge

platform during modal testing. In the analysis the bearing support stiffness of $K_B=100\ N/m$ has been used for each bearing, and all shaft connections and link boltings have been assumed as continuous solid connections.

Analytical natural frequencies of the bending modes for the single and dual shaft models, excluding those of the 1st and 2nd rigid body modes, are presented in Table 1 along with the modal test results. For the single shaft model, the 3rd (so called the 1st bending mode) natural frequency is 59,110 rpm, and the 4th and 5th are 137,262 and 245,904 rpm. The analytical and test results agree with each other to within 4% difference. And it has been confirmed that there is no practical effect of the inner shaft tension of 50,000 N on the system natural frequencies for this modeling case.

For the dual shaft model with no inner shaft tension considered, natural frequencies of the bending modes are 60,759, 137,788, and 252,197 rpm for the outer-shaft-modes and 41,275, 103, 369, and 219,908 rpm for the inner-shaft-modes.

Table 1 Analysis versus modal test results of the mock-up APU rotor (%: the difference between the analysis and modal test results)

Analytical results Natural frequency (rpm)			Modal test results (rpm)	Dominant mode
Single shaft model	Dual shaft model			
	With no axial force	With axial force		
	41,275	46,994		Inner shaft
59,110 (+0.9%)	60,759 (+3.8%)	60,832 (+3.9%)	58,560	Outer shaft
	103,369	112,728		Inner shaft
137,262 (+3.4%)	137,788 (+3.8%)	137,941 (+3.9%)	132,720	Outer shaft
	219,908	229,673		Inner shaft
245,904 (+2.1%)	252,197 (+4.7%)	252,556 (+4.8%)	240,960	Outer shaft

The outer-shaft-mode natural frequencies of the dual shaft model have increased 0.4~2.5%, compared to those of the single shaft model, and they agree with the test results to within 5% difference. With the inner shaft tension considered the outer-shaft-mode natural frequencies have increased a little (up to +0.1%), compared to those with no tension considered. But with the inner shaft tension considered the inner-shaft-mode natural frequencies have increased 4.4~13.9%, compared to those with no tension considered.

From the above results it can be stated that all shaft connections and link boltings in the APU rotor may be treated as continuous solid connections, and that the present dual shaft model is good enough to yield accurate results for the main outer-shaft-modes to within 5% error, along with prediction capabilities of the inner-shaft-modes.

3.2 Prototype APU rotor-bearing system

Figures 1 and 4 show a schematic of the prototype APU rotor and its equivalent finite element model. Two air foil bearing locations are marked in Fig. 4 as the hatched triangle supports. Applying the foregoing single and dual shaft models detailed whirl mode and unbalance response analyses have been carried out with the prototype APU rotor-bearing system. In the analyses the following air-foil bearing dynamic coefficients have been used: $K_B=2\times10^6\ N/m$ and $C_B=1\times10^3\ N\cdot s/m$ for the LHS bearing, and $K_B=8\times10^6\ N/m$ and $C_B=2\times10^3\ N\cdot s/m$ for the RHS bearing.

3.2.1 Whirl mode shapes and critical speeds

For the single shaft model, critical speeds are given in Table 2, where the effect of the inner shaft tension of 50,000 N has not been considered in this analysis. The 1st and 2nd modes have the

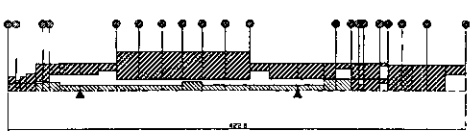

Fig. 4 An equivalent finite element model of the prototype APU rotor

Table 2 Rotordynamic analysis results of the prototype APU rotor-bearing system, depending on the different modeling approaches

Analytical Results Critical speed (rpm)			Dominant mode
Single shaft model	Dual shaft model		
	With no axial force	With axial force	
5,801	5,799	6,015	Rigid body
8,030	8,028	8,027	Rigid body
	40,314	56,184	Inner shaft bending
82,802	82,996	83,019	Outer shaft bending
	118,409	142,665	Inner shaft bending
173,815	174,420	174,470	Outer shaft bending

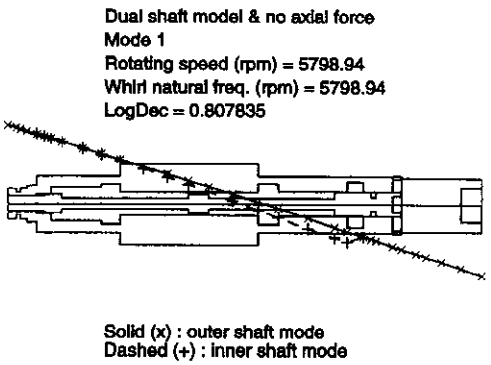

Fig. 5 1st critical mode of the APU rotor for the dual shaft model

same shapes as the outer-shaft-modes in Figs. 5 and 6 at the 1st and 2nd criticals for the dual shaft model. They are rigid body modes, and have the critical speeds of 5,801 and 8,030 rpm. The 3rd mode has the same shape as the outer-shaft-mode in Fig. 8 at the 4th critical for the dual shaft model. It is a bending mode, and has the critical speed of 82,802 rpm. As the APU has the rated speed of 60,000 rpm, the 3rd critical speed has the sufficient separation margin.

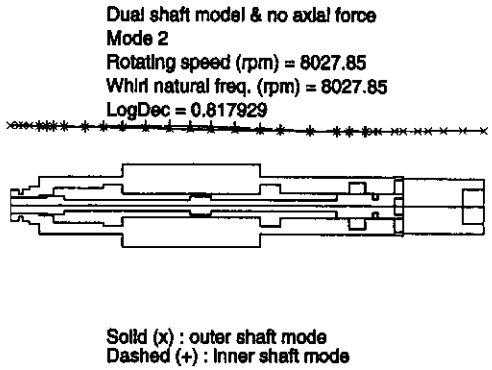

Fig. 6 2nd critical mode of the APU rotor for the dual shaft model

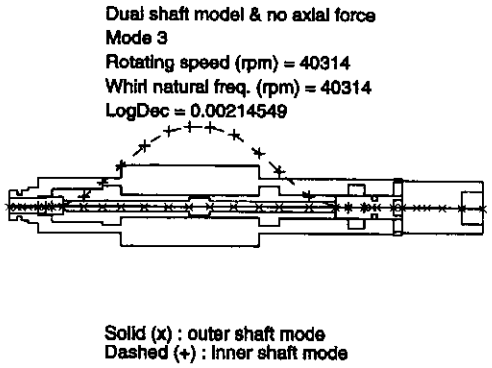

Fig. 7 3rd critical mode (inner-shaft-mode) of the APU rotor for the dual shaft model

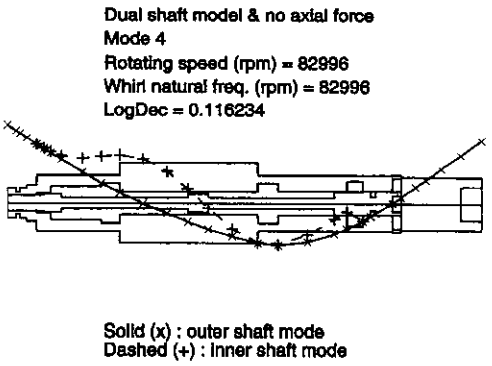

Fig. 8 4th critical mode (outer-shaft-mode) of the APU rotor for the dual shaft model

For the dual shaft model with no inner shaft tension considered, whirl mode analysis results are shown in Figs. 5~9. The 1st and 2nd modes have the critical speeds of 5,799 and 8,028 rpm. They are practically the same as those for the

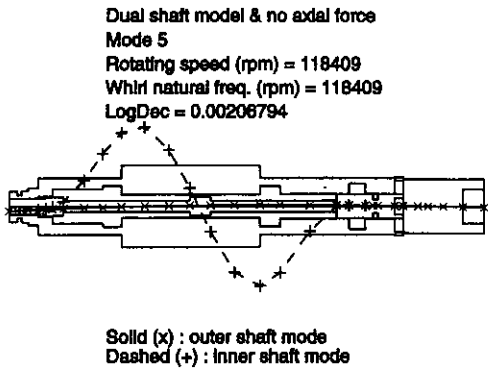

Fig. 9 5th critical mode (inner-shaf-mode) of the APU rotor for the dual shaft model

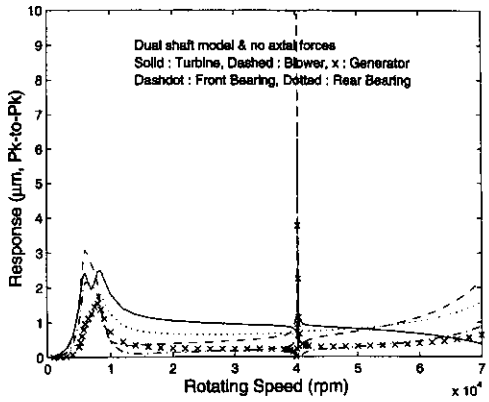

Fig. 10 Unbalance response at the outer shaft of the APU rotor for the full speed range for the dual shaft model

single shaft model. For the 3rd mode in Fig. 7 and 5th mode in Fig. 9 the inner shaft is greatly excited whereas the outer shaft excitation is little. Therefore, they are the inner shaft bending modes. Their critical speeds are 40,314 and 118,409 rpm. Here, since the 3rd critical speed is within the operating speed range and its LogDec (Logarithmic Decrement) is very low, its effect needs to be further investigated by unbalance response analysis. On the other hand, the 4th mode in Fig. 8 is the outer shaft bending mode. Its critical speed is 82,996 rpm, which is very close to that of the 3rd mode for the single shaft model.

In Table 2 summarized are the critical speeds obtained for the various modeling cases. For the dual shaft model with the inner shaft tension considered, the 3rd and 5th critical speeds due to the inner shaft bending modes increase greatly. Particularly the 3rd critical speed is predicted as 56,184 rpm, which are very close to the rated speed. Therefore, this 3rd critical speed effect also needs to be further investigated by unbalance response analysis.

3.2.2 Unbalance responses

Unbalance response analyses have been performed with magnitude twice the API allowable residual unbalance limit, which have been attached to the generator and turbine by 0.564 g · mm and 2.328 g · mm, respectively, in-phase.

For the single shaft model, unbalance response has been predicted to be quite satisfactory, having less than 4 μm Pk-to-Pk vibrations at the rated

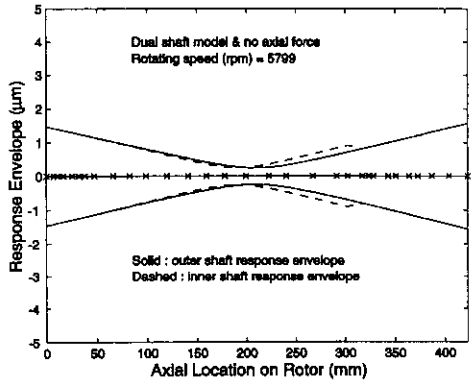

Fig. 11 Unbalance response at the 1st rigid-mode critical speed of the APU rotor for the dual shaft model

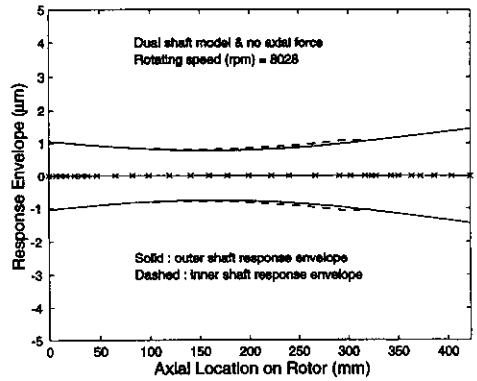

Fig. 12 Unbalance response at the 2nd rigid-mode critical speed of the APU rotor for the dual shaft model

speed of 60,000 rpm and at the two passing

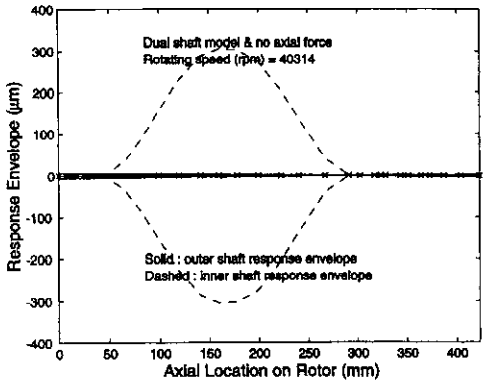

Fig. 13 Unbalance response at the 3rd inner shaft critical speed of the APU rotor for the dual shaft model

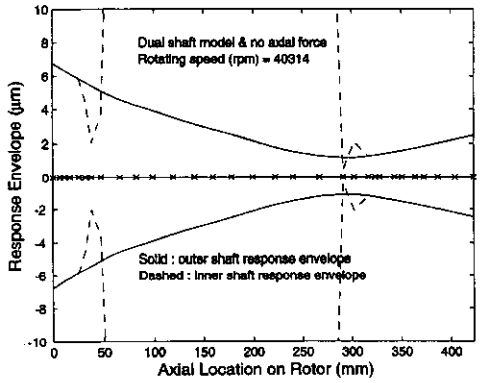

Fig. 14 Close-up view of the unbalance response at the 3rd inner shaft critical speed of the APU rotor for the dual shaft model

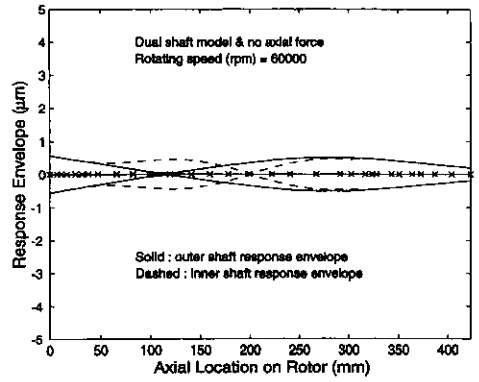

Fig. 15 Unbalance response at the rated speed of 60,000 rpm of the APU rotor for the dual shaft model

critical speeds of rigid body modes.

For the dual shaft model with no inner shaft tension considered, unbalance response analysis results are shown in Figs. 10~15. Unbalance response characteristic of the outer main rotor shaft is given for 0 to 70,000 rpm range with coarse rpm steps in Fig. 10. Three response peaks are observed due to the two rigid body modes and one inner shaft bending mode criticals. Figures 11 and 12 show unbalance responses at the 1st and 2nd criticals. The responses throughout the entire rotor locations are all less than 4 μm Pk-to-Pk. Figure 13 shows unbalance response at the 3rd critical speed of the inner shaft bending mode. Due to the inner shaft resonance the inner shaft response, which is marked as a dashed line, can reach as high as 600 μm Pk-to-Pk. A magnified view in Fig. 14 shows that the outer shaft response can grow up to 13 μm Pk-to-Pk due to the influence of the inner shaft resonance. This outer shaft vibration level could be concern as the rotor journals supported by the air-foil bearings operate on very thin air film. Figure 15 shows unbalance response at the rated speed, and vibration level is predicted as less than 2 μm Pk-to-Pk.

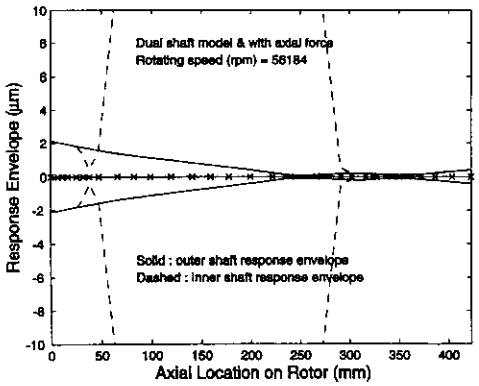

Fig. 16 Close-up view of the unbalance response at the 3rd inner shaft critical speed of the APU rotor for the dual shaft model and axial force considered

For the dual shaft model with the inner shaft tension considered, unbalance responses at the 1st and 2nd criticals all have been less than 4 μm Pk-to-Pk, again. However, at the 3rd critical speed of the inner shaft bending mode the inner shaft response can increase as high as 200 μm Pk-to-Pk, and the outer shaft response can grow up to a

little over 4 μm Pk-to-Pk as shown in Fig. 16, again due to the influence of the inner shaft resonance.

From the above results it can be stated that the single and dual shaft models applied to the prototype APU rotor-bearing system may produce practically the identical mode shapes and critical speeds for the outer main rotor shaft. However, that the dual shaft model additionally and more importantly can predict the inner shaft behavior at the concerned 3rd critical speed and its effect on the rotordynamic characteristics of the entire APU rotor-bearing system. On the other hand, since the boundary conditions at the contact points (or common nodes) of the inner tie shaft to the inside of the outer shaft are short of a perfect fixed boundary, it is more reasonable that the 3rd critical speed of the inner shaft bending mode would be closer to the one predicted with no inner shaft tension considered rather than the other.

4. Conclusions

The main purpose of the present study is to set-up an accurate model of the prototype APU rotor system and particularly to investigate the influences of the tie shaft on the rotordynamic characteristics of the entire APU rotor-bearing system. Firstly, for the mock-up APU rotor, comparisons of modal test and analytical results have shown that all shaft connections and link boltings may be treated as continuous solid connections, and that the dual shaft model is good enough to yield accurate results to within 5% error for the outer main rotor shaft modes. Then, for the prototype APU rotor-bearing system, the dual shaft model proposed has shown that the APU system has one inner shaft bending mode critical speed before it reaches its rated speed of 60,000 rpm, which has not been predicted by the conventional single shaft model. Unbalance analysis results have shown that the outer main rotor shaft may have some amplified responses due to the inner shaft resonance at the 3rd critical speed. This amplified outer shaft vibration could be concern as the rotor journals supported by the air-foil bearings operate on very thin air film. It is concluded as a conservative design practice that the inner tie shaft should be explicitly modeled in the rotordynamic analysis of the APU rotor-bearing system, and that its effects on the dynamic behaviors of the main outer shaft should be thoroughly reviewed during design stage.

References

Janssen, M. J. and Joyce, J. S., 1996, "35-Year Old Splined-Disc Rotor Design for Large Gas Turbines," ASME Paper 96-GT-523 presented at the International Gas Turbine and Aeroengine Congress & Exhibition, June 10-13, Birmingham, U. K.

Koenig, E. C., 1961, "Analysis for Calculating Lateral Vibration Characteristics for Rotating Systems With Any Number of Flexible Supports," *ASME Trans., Journal of Applied Mechanics*, pp. 585~590.

Lalanne, M. and Ferraris, G., 1990, *Rotordynamics Prediction in Engineering*, John Wiley and Sons.

Lund, J. W. and Orcutt. F. K., 1967, "Calculations and Experiments on the Unbalance Response of a Flexible Rotor," *ASME Trans., Journal of Engineering for Industry*., pp. 785~796.

Özgüven, H. N. and Özkan Z. L., 1984, "Whirl Speeds and Unbalance Response of Multibearing Rotors Using Finite Elements," *ASME Trans., Journal of Vibration, Acoustics, Stress, and Reliability in Design*, Vol. 106, pp. 72~79.

Pestel, E. C. and Leckie, F. A., 1963, *Matrix Methods in Elasto Mechanics*, McGraw-Hill Book Co., Inc.

Rao, J. S., 1983, *Rotor Dynamics*, A Halsted Press Book.

Ruhl, R. L. and Booker, J. F., 1972, "A Finite Element Model for Distributed Parameter Turborotor Systems," *ASME Trans., Journal of Engineering for Industry*, pp. 126~132.

Zorzi, E. S. and Nelson, H. D., 1977, "Finite Element Simulation of Rotor-Bearing Systems with Internal Damping," *ASME Trans., Journal of Engineering for Power*, Vol. 99, pp. 71~76.

Appendix

Referring to Fig. 2, displacements at any location along a shaft element is expressed as functions of its corresponding generalized nodal displacements, $\{q_i\}$, at the both ends through the shape functions. The kinetic energy of the shaft element is expressed as

$$T_S=\frac{1}{2}\rho\int_0^l A(\dot{u}^2+\dot{v}^2)dZ+\frac{1}{2}\rho\int_0^l I_t(\dot{\theta}_X{}^2+\dot{\theta}_Y{}^2)dZ$$
$$-\rho\Omega\int_0^l I_p\dot{\theta}_Y\theta_X dZ+\frac{1}{2}\rho\Omega^2\int_0^l I_p dZ \qquad (A1)$$

where ρ is a density, A is a cross sectional area, I_t and I_p are transverse and polar area moments of inertia, and Ω is a rotating speed. The strain energy of the shaft element is expressed as

$$U_S=\frac{1}{2}E\int_0^l I_t\left[\left(\frac{\partial^2 u}{\partial Z^2}\right)^2+\left(\frac{\partial^2 v}{\partial Z^2}\right)^2\right]dZ \qquad (A2)$$

where E is a modulus of elasticity. The kinetic energy of a lumped disk is expressed as

$$T_D=\frac{1}{2}m_D(\dot{u}^2+\dot{v}^2)+\frac{1}{2}I_{Dt}(\dot{\theta}_X{}^2+\dot{\theta}_Y{}^2)$$
$$-I_{Dp}\Omega\dot{\theta}_Y\theta_X+\frac{1}{2}I_{Dp}\Omega^2 \qquad (A3)$$

where m_D, I_{Dt}, and I_{Dp} are a mass and transverse and polar moments of inertia of the disk. The equations of motion of each shaft and disk elements are obtained by applying the following Lagrange's equation to Eqs. (A1~3).

$$\frac{d}{dt}\left(\frac{\partial T}{\partial\dot{q}_i}\right)-\frac{\partial T}{\partial q_i}+\frac{\partial U}{\partial q_i}=Q_i \qquad (A4)$$

where Q_i is the generalized applied force in the q_i direction. Stiffness and damping forces of support bearings, unbalance excitation forces, and other generalized forces, including rotor gravity forces, at any node may be obtained by introducing the virtual work concept. The virtual work at a certain node is expressed as

$$\delta W=Q_u\delta u+Q_v\delta v+Q_{\theta X}\delta\theta_X+Q_{\theta Y}\delta\theta_Y$$
$$=[Q_i]\{\delta q_i\} \qquad (A5)$$

where Q_u, Q_v, $Q_{\theta X}$, and $Q_{\theta Y}$ are the generalized forces in the corresponding nodal displacement directions. After assembling the equations of motion of component elements, constituting the entire rotor-bearing system, the resultant global system equations of motion can be expressed in the form

$$[M]\{\ddot{q}\}+[C]\{\dot{q}\}+[K]\{q\}=\{Q\} \qquad (A6)$$

where $[M]$, $[C]$, and $[K]$ are the global mass, damping, and stiffness matrices. The gyroscopic components are included in $[C]$.

For free vibration analysis Eq. (A6) may be expressed in the state-space form as

$$\begin{Bmatrix}\{\dot{q}_2\}\\ \{\dot{q}_1\}\end{Bmatrix}=[A]\begin{Bmatrix}\{q_2\}\\ \{q_1\}\end{Bmatrix},\ with\ \begin{matrix}\{q_1\}=\{q\}\\ \{q_2\}=\{\dot{q}\}\end{matrix} \qquad (A7)$$

where $[A]$ is the dynamic matrix of the system. It is defined as

$$[A]=\begin{bmatrix}-[M]^{-1}[C] & -[M]^{-1}[K]\\ [I] & [0]\end{bmatrix} \qquad (A8)$$

The eigenvalues and eigenvectors are calculated from the dynamic matrix to give whirl natural frequencies and mode shapes. Unbalance response of the system is derived by substituting the following generalized unbalance force and assumed solution into Eq. (A6):

$$\{Q\}=\Omega^2\{U_C\}\cos\Omega t+\Omega^2\{U_S\}\sin\Omega t \qquad (A9)$$
$$\{q\}=\{a\}\cos\Omega t+\{b\}\sin\Omega t \qquad (A10)$$

where $\{U_C\}$ and $\{U_S\}$ are the coefficient vectors of unbalance forcing, and $\{a\}$ and $\{b\}$ are the coefficient vectors of unbalance solution. After some algebraic manipulations the following unbalance matrix equation is obtained:

$$\begin{bmatrix}[K]-\Omega^2[M] & \Omega[C]\\ -\Omega[C] & [K]-\Omega^2[M]\end{bmatrix}\begin{Bmatrix}\{a\}\\ \{b\}\end{Bmatrix}=\Omega^2\begin{Bmatrix}\{U_C\}\\ \{U_S\}\end{Bmatrix} \qquad (A11)$$

Then, $\{a\}$ and $\{b\}$ of the unbalance response are calculated from Eq. (A11).